Understanding Chemical Ordering in Bimetallic Nanoparticles from Atomic Scale Simulations: The Competition between Bulk, Surface and Strain

J. Magnus Rahm and Paul Erhart*

Chalmers University of Technology, Department of Physics, S-412 96 Gothenburg, Sweden

E-mail: erhart@chalmers.se

Abstract

Bimetallic nanoparticles are highly relevant for applications in, e.g., catalysis, sensing, and energy harvesting. Their properties are determined by their shape, size, and, most notably, their chemical configuration, i.e., the elemental distribution throughout the particle. To fully exploit their potential a comprehensive understanding of the coupling between size, shape, and chemical ordering is crucial. Here, we employ hybrid molecular dynamics–Monte Carlo simulations to reveal the energetics of two prototypical nanoalloys, Ag–Cu and Au–Pd, by comprehensive sampling across the full composition range, while considering both size and shape as parameters. Our simulations expose the interplay between bulk thermodynamics, surface energetics and strain. Relative to the bulk, the behavior of Au–Pd nanoalloys is dominated by surface segregation, and is thus largely independent of particle size and shape. By contrast, strain plays a key role in the Ag–Cu system, whence size and, even more so, shape have a strong impact on the overall energetics and accordingly the elemental distribution. This effect is reflected by the sign of the mixing energy curve, which in the case of the Ag–Cu system changes from positive to negative when going from the bulk to the nanoscale. While this suggests miscibility it is rather a manifestation of segregation to different sites.

Graphical TOC Entry

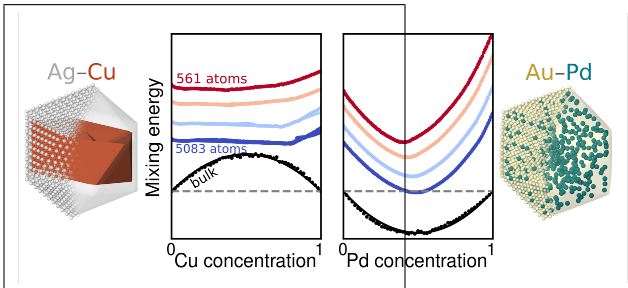

Introduction

All monometallic nanoparticles are alike; each bimetallic nanoparticle is ordered in its own way. Chemical ordering, i.e., the arrangement of different species within a nanoparticle, together with size, shape and average composition has a profound influence on optical, catalytic and numerous other properties.[1–6] While thermodynamics provides the ultimate driving forces for elemental distribution, kinetic barriers can be exploited to grow particles with very tailored (and far-from-equilibrium) elemental distributions.[7–9] Nanoalloys thus provide tremendous possibilities for optimization for specific applications. To this end, it is, however, crucial that the chemical ordering in thermodynamic equilibrium be understood and reliably predicted over a wide range of sizes, shapes, and compositions.

Phase diagrams for bulk alloys provide information that also have a bearing at the nanoscale.[10] In a binary alloy that segregates into almost pure phases, for example, the low solubility of either element in the other is the signature of the interaction between unlike atoms being less favorable than the interaction between alike atoms. Such a characteristic cannot be expected to change dramatically at smaller length scales, and we should thus expect segregation in the nanoalloy as well. At the nanoscale, however, it is necessary to also take into account surfaces, strain and other defects. If the surface energies of the constituent elements differ, we would expect the element with the lower surface energy to segregate to the surface. If there is a size mismatch between the elements, we would expect the smaller element to segregate to compressively strained parts of the particle.

The chemical ordering in nanoparticles is thus determined by the competition between bulk-like chemical interaction, surface segregation, and strain-driven segregation. Since these contributions scale differently with particle dimension, chemical ordering is bound to be affected by size.[11,12] The surface-to-volume ratio and, even more so, strain are furthermore sensitive to shape, which thus constitutes an additional variable.[13,14] Chemical ordering is thus the result of an interplay of contributions that vary from alloy to alloy and depend on both size and shape.[11,14–18]

This interplay has been illuminated with theoretical studies based on continuum modeling[19] with focus on both surface[20–22] and strain effects.[23] Continuum models naturally lend themselves to exhaustive studies of the full composition range over large size ranges. They are, however, prone to miss out on the finer details of chemical ordering on the atomic scale. This aspect can instead be approached with atomic scale modeling, which is, however, computationally much more expensive and thus challenging to apply to a wide range of compositions, sizes and shapes. Atomic scale modeling of nanoalloys requires particular attention to two sets of degrees of freedom: atomic positions and chemical configuration. Because the number of degrees of freedom grows very quickly with particle size, searches for energy minima in particles that are larger than a few hundred atoms are inevitably restricted in at least one of the two sets of degrees of freedom. When restrictions are imposed, one will thus sample local minima. From a practical standpoint these are, however, just as important as particles experimentally are almost always found off-equilibrium, in local minima that are bound by very substantial energy barriers.[24] This realization has motivated a multitude of studies with different approaches, including genetic algorithms and basin hopping[25,26] as well as molecular dynamics (MD) and Monte Carlo (MC) simulations.[13,27–31]

In this work, we use an efficient computational technique based on a combination of MD and MC simulations in a variance-constrained ensemble to comprehensively sample nanoparticles of many sizes and shapes across the full concentration range. The MC component allows for an unrestricted search through the space of chemical configurations, whereas MD allows for sampling of atomic positions in the vicinity of the atomic positions defined at outset of the simulation. The particles are thus restricted to retain their shape (structural motif) throughout the simulations. With this method, we are able to illustrate the competition between bulk-like interactions, surface segregation and strain-driven segregation as a function of both size and shape with and without temperature. We consider gold–palladium (Au–Pd) and silver–copper (Ag–Cu) nanoalloys as two prototypical alloys that exhibit opposing extremes. Au–Pd mixes in the bulk and has a relatively small size mismatch, whereas Ag–Cu has a wide miscibility gap and a large size mismatch. The surface energies differ substantially between the two elements in both alloys. As a result of these differences these systems are well suited for investigating the impact of surface segregation and strain.

We show that in the case of Ag–Cu the shape of the mixing energy curve, an important quantity for predicting segregation, is inverted when going from bulk to the nanoscale and discuss the consequences thereof. Comprehensive sampling also allows us to discover ground state chemical configurations that are more revealing than previously reported. For segregating systems, computational studies have generally found that the energetically most favorable particle has a core–shell structure, possibly with the core positioned off-center.[16,29,32–34] Here, we show that while this is often the case, the notion of a core surrounded by a shell is to some extent misleading, since the shape of the segregate is largely governed by the structural motif and may at some compositions attain highly symmetric, e.g., ring-like, configurations that cannot be described as core–shell.

Methods

The thermodynamic properties of Ag–Cu and Au–Pd nanoalloys were studied as a function of size and shape using a hybrid MD–MC algorithm based on the variance-constrained semi-grandcanonical (VCSGC) ensemble[35,36] as implemented in LAMMPS.[37] For a two-component (binary) system with components A and B composed of N particles where c is the concentration of species B the partition function of the VCSGC ensemble is given by[35,36]

$$\mathcal{Z}_{\mathrm{V}} = \int_0^1 dc \mathcal{Z}_{\mathrm{C}}(c, N, V, E) \exp\left[-\beta\bar{\kappa}N\left(c+\bar{\phi}/2\right)^2\right]. \tag{1}$$

Here, $\mathcal{Z}_{\mathrm{C}}$ is the canonical partition function and $\beta = 1/k_B T$, while $\bar{\phi}$ and $\bar{\kappa}$ are two parameters that constrain the average and the variance of the concentration c, respectively.[1] Unlike the semi-grandcanonical (SGC) ensemble the VCSGC ensemble enables one to sample the system also inside miscibility gaps, i.e. concentration regions in which the mapping between the chemical potential difference and the concentration is not one-to-one.

---

[1] We use the effective parameters $\bar{\phi}$ and $\bar{\kappa}$, which were introduced in Sect. II.C of Ref.[36] and are more convenient in practice than the original parameters ϕ and κ.

In the present work, we sequentially varied $\bar{\phi}$ in steps of 0.02 from -2.2 to 0.2 and vice versa, effectively switching the system from pure Ag/Au to pure Cu/Pd and the other way around. The variance constraint parameter $\bar{\kappa}$ can be chosen from a rather wide range covering approximately two orders of magnitude.[36] Here, we adopted a value of $\beta\bar{\kappa} = 500$ throughout, which provides a good compromise between the strength of the constraint and the acceptance rate.

To optimize the chemical ordering at zero temperature, we conducted simulated annealing runs in which the sequential variation of $\bar{\phi}$ was combined with a gradual reduction of the temperature from 500 K to 200 K at a rate of 1,000 MD steps/K, followed by a conjugate gradient minimization of the structure. During the MD sequence the temperature in the system was controlled using a Nosè-Hoover thermostat. Every 100 MD steps, the MD simulation was interrupted to carry out a full cycle of VCSGC MC trial moves[2]. Simulations were carried out for nanoparticles of different size and shape as well as slabs with 25 atomic layers.

In addition to simulated annealing, simulations were conducted in which the sequential variation of $\bar{\phi}$ described above was carried out at a fixed temperature. In these runs, 40% of a full MC sweep was performed every 100 MD steps. At each $\bar{\phi}$ value the system was equilibrated for 1,000 MD steps, after which statistical averages were generated over 100,000 MD steps.

Throughout this work, the potential energy E was calculated using embedded atom method (EAM) potentials parametrized by Mishin *et al.*[38] and Williams *et al.*[39] for Ag–Cu, and Marchal *et al.*[40] for Au–Pd. Calculations of the volumetric strain as well as visualization were carried out using OVITO.[41]

Results and discussion

We define the mixing energy as

$$E_{\text{mix}} = E_{\text{A–B}} - cE_{\text{A}}^{\text{bulk}} - (1-c)E_{\text{B}}^{\text{bulk}}, \tag{2}$$

---

[2] 1 cycle is here defined as N trial moves where N is the total number of atoms.

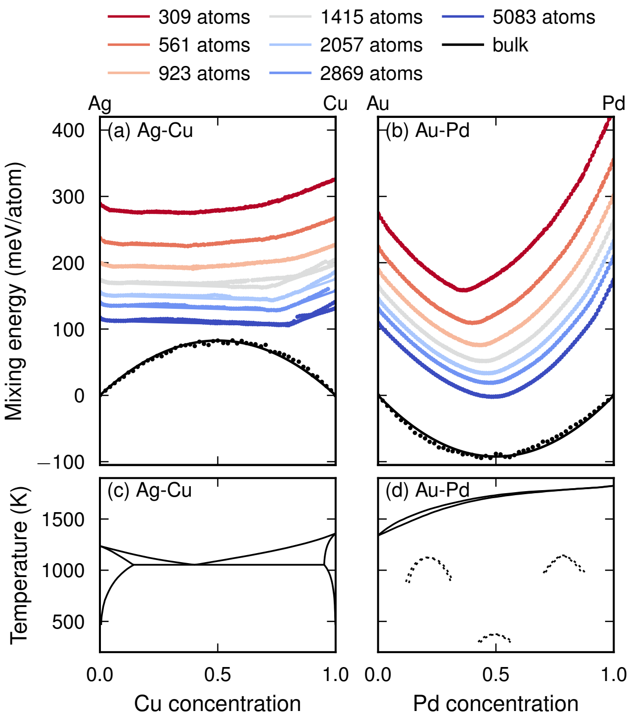

Figure 1: Mixing energy at 0 K in icosahedral (a) Ag–Cu and (b) Au–Pd nanoalloys as obtained from simulated annealing runs (colored lines), compared to random bulk configurations of the respective binary system (black). Two simulations were carried out for each size, one starting with pure Ag/Au and ending with pure Cu/Pd and one in the opposite direction. The lower row shows experimental bulk phase diagrams for (c) Ag–Cu[42] and (d) Au–Pd.[43]

where $E_{\mathrm{A–B}}$ is the energy per atom of the alloy system and c the concentration of A atoms. In the present work, the reference energy $E_{\mathrm{X}}^{\mathrm{bulk}}$ is chosen to refer to the energy per atom of species X in the *bulk*. This quantity highlights the effect of surface and strain energy contributions on the pure nanoparticles. We note that E_{mix} is always positive for Ag–Cu in *bulk*, leading to separation into Ag-rich and Cu-rich phases (Fig. 1c). For Au–Pd, on the other hand, E_{mix} in bulk is always negative, leading to complete mixing, possibly with ordered intermetallic phases at lower temperatures (Fig. 1d).

For nanoparticles (Fig. 1a–b) the situation is slightly more intricate. Both Ag–Cu and Au–Pd have positive E_{mix}, primarily because of the surface energy since in general nanoparticles are energetically unfavourable relative to the bulk. Interestingly, the mixing energy curves are, however, convex not only for Au–Pd but also for Ag–Cu. The behaviour is the same in particles with icosahedral, truncated octahedral and decahedral shape (Fig. S1 of the Supporting Information). The inversion of the shape of the mixing energy curve for Ag–Cu implies that mixed particles are energetically preferable over pure ones in contrast to the bulk case. It should not, however, be interpreted as a sign for the formation of a mixed phase as it would in a bulk system. Rather, the system segregates in a way that leads to a substantial lowering of the energy. This behavior is possible since some of the energy penalties related to the nanoscale, most notably surface and strain energy, can be relieved if the different species segregate to sites that are favourable for the respective element as will be elaborated in the following.

Ag has a lower surface energy than Cu (54 and 77 meV/Å^2 for the $\{111\}$ facet, respectively, as calculated with the present EAM potential; 77 and 111 meV/Å^2 experimentally[44]) and Au has lower surface energy than Pd (48 and 85 meV/Å^2, respectively, as calculated with the present EAM potential; 94 and 125 meV/Å^2 experimentally[44]). The energy is therefore lowered if Ag segregates to the surface of the Ag–Cu particles and Au to the surface of Au–Pd particles. It should be noted that this behavior corresponds to vacuum conditions. Adsorbates can have a pronounced effect on surface energetics and invert segregation tendencies.[45]

The slopes of the mixing energy curves in the Cu-rich and Pd-rich limits are essentially independent of size (Fig. S2 of the Supporting Information). The gain in mixing energy due to addition of Ag to the surface of a pure Cu particle is about 0.1 eV/atom. This value is lower than what would be expected from the difference in Ag and Cu surface energies, highlighting that the dissimilar bonds between the Ag surface and Cu subsurface are associated with an energy penalty. The energy gain of putting Au in the surface of a pure Pd particle is about 0.64 eV/atom, which, because of the mixing tendencies of Au–Pd, is more than what would be expected from the difference in surface energies.

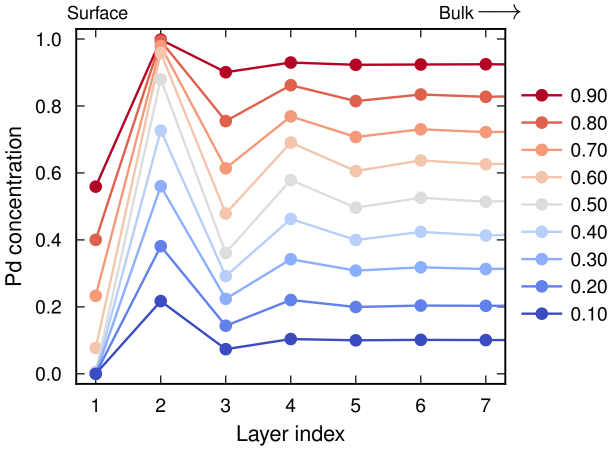

Figure 2: Concentration of Pd per atomic layer in a Au–Pd slab with 25 atomic layers terminated with a $\{111\}$ facet, at 300 K. Only the seven topmost layers are shown here, with layer 1 being the surface layer. The labels indicate Pd concentration in the system as a whole.

Surface segregation is not limited to nanoparticles but is observed also for flat surfaces (Fig. 2). Here, it is noteworthy that the segregation of Pd to the first subsurface layer of a Au–Pd slab is almost as strong as the segregation of Au to the surface layer. In fact, the concentration profile exhibits an oscillatory behavior, with layers alternatingly enriched in Au and Pd, until the effect fades out a few atomic layers into the slab. We attribute this effect to the favorable energy of the Au–Pd bond, compared to Au–Au and Pd–Pd. The surface thus has an impact on the subsurface mediated by bulk-like chemical bonds. The Ag–Cu system does not straightforwardly lend itself to the same analysis, since segregation induces surface reconstruction and introduces spurious size effects.

We observe the same behavior, i.e., Au enriched surface layer and alternatingly enriched subsurface layers, also in Au–Pd nanoparticles at 300 K (Fig. 3a). Particles of this kind have been observed also in previous studies[40] and are sometimes referred to as onion-like.[1] The concentration profile is also isotropic and essentially identical regardless of particle size and shape (Fig. 4, Figs. S4–6 of the Supporting Information). In conclusion, the equilibrium chemical configuration of Au–Pd particles is driven primarily by the bulk-like chemical bonds and surface segregation, and is essentially the same in a surface slab and in a particle.

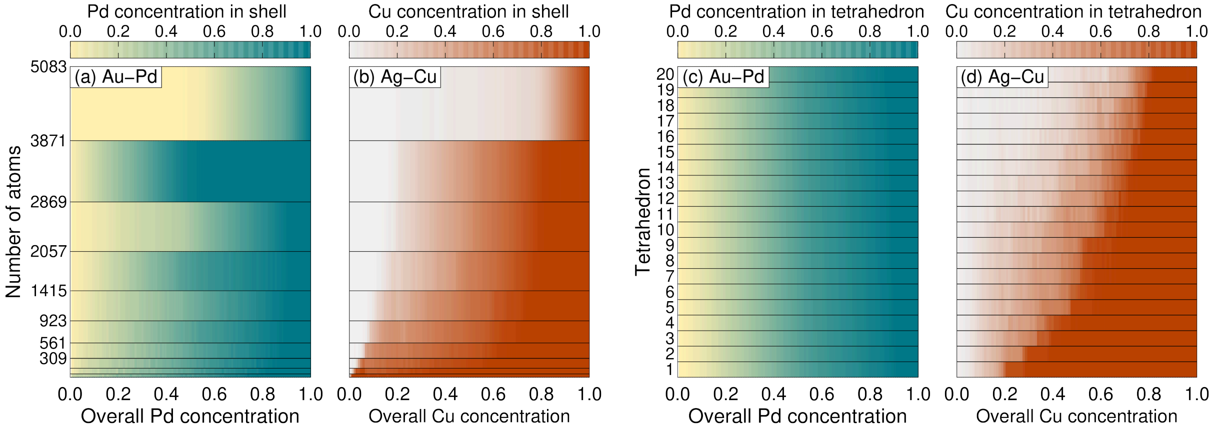

Figure 3: Average concentration at 300 K in icosahedral Au–Pd (left) and Ag–Cu (right) particles with 5,083 atoms, ordered by (a–b) atomic shell, with core at the bottom and surface at the top, and (c–d) tetrahedra, excluding the innermost 55 atoms as well as the faces of each tetrahedron (leaving 120 atoms per tetrahedron). The tetrahedra are ordered by concentration. The horizontal axes represent the overall Pd/Cu concentration in the particle as a whole whereas the color scale represents the concentration in each shell/tetrahedron specifically.

While bulk-like contributions are naturally also present in the Ag–Cu system, strain plays a much more dominant role than in the case of Au–Pd due to the pronounced size mismatch. Bulk Cu has a substantially smaller lattice parameter than Ag (3.615 Å and 4.09 Å for Cu and Ag, respectively, as calculated with the present EAM potential), meaning that strain energy may be relieved if Cu is placed in regions under compression. The strain field is, however, to a large extent dependent on the underlying structural motif of the particle, and as a consequence, the preferential positions of the Cu atoms within the particle must be analyzed for each structural motif separately. Here, we consider icosahedral, truncated decahedral and truncated octahedral particles, all of which have been shown to be thermodynamically favorable for noble metal particles in the small or medium

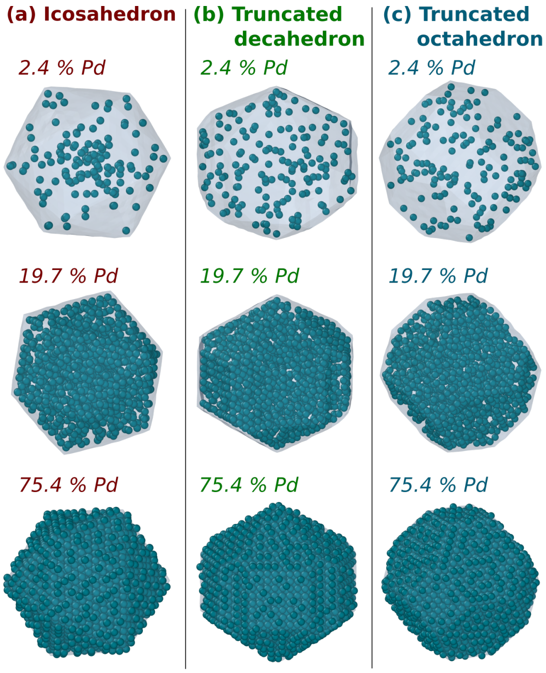

Figure 4: Representative snapshots of Au–Pd particles at 300 K, 5,083 atoms icosahedral (left) 6,593 atoms truncated decahedral (middle) and 6,266 regular truncated octahedral (right). The uppermost row shows the volumetric strain in relaxed particles of pure Ag.

size regime.[46]

Icosahedral particles (Fig. 5) can be thought of as twenty face-centered cubic (FCC) tetrahedra stacked together so that they all share an atom in the center of the particle while every two neighboring tetrahedra share a common face, forming a twin boundary. The particle has a low surface-to-volume ratio for its size and only $\{111\}$ facets. It is, however, geometrically impossible to construct without straining the constituent tetrahedra, resulting in a highly compressed core (Fig. 5a, top row). Accordingly, Cu has a strong tendency to segregate to the core of icosahedral particles (Fig. 5a, second row). This is particularly striking when the Cu concentration is represented atomic layer by layer (Fig. 3b). Naively, one might expect that in going from a pure Ag particle to pure Cu there should be an isotropically growing Cu core surrounded by an Ag shell; this is, however, not observed. As the core has reached a certain size (dependent on overall particle size), the Cu segregate starts to grow anisotropically. In going from pure Ag to pure Cu, the constituent tetrahedra tend to switch from Ag to Cu one by one (Fig. 3b), akin to previous experimental observations of sequential hydride formation in Pd icosahedra.[47] This behavior is

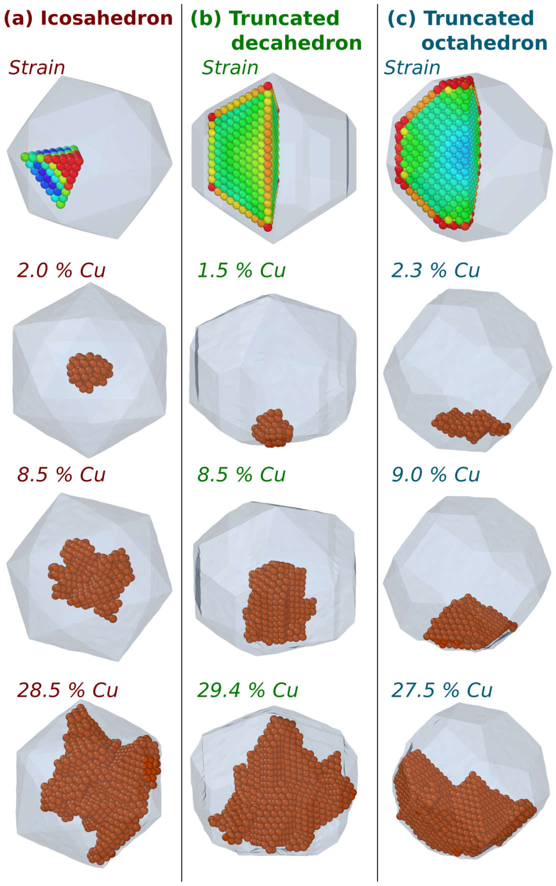

Figure 5: Representative snapshots of Ag–Cu particles at 300 K, 5,083 atoms icosahedral (left) 6,593 atoms truncated decahedral (middle) and 6,266 regular truncated octahedral (right).

particularly striking in small particles subjected to simulated annealing (Fig. 6) but to some extent also occurs in particles with several thousand atoms and at elevated temperatures. The shape of the Cu segregate is thus dictated by which tetrahedra have switched and which have not. A particularly stable structure, at least for particles with less then a few thousand atoms, is formed when ten tetrahedra have switched to Cu and ten are still Ag. The Cu tetrahedra then arrange in a ring sandwiched between two caps of Ag (Fig. 6c). This sandwich-like particle can hardly be described as core–shell. For other compositions the segregate is typically less symmetric. In some cases the Cu tetrahedra cluster together forming what previous simulation studies at fixed concentrations reported as off-center cores.[28,33,34] More often the segregates are spread out in the particle, separated by tetrahedra that predominantly contain Ag (Fig. 5a, fourth row). Note that these types of behavior are in stark contrast to Au–Pd particles with the same shape, for which the distribution is completely isotropic (Fig. 3c). Note also that these particles generally have a large Ag–Cu interface area in contrast to what is expected in bulk Ag–Cu.

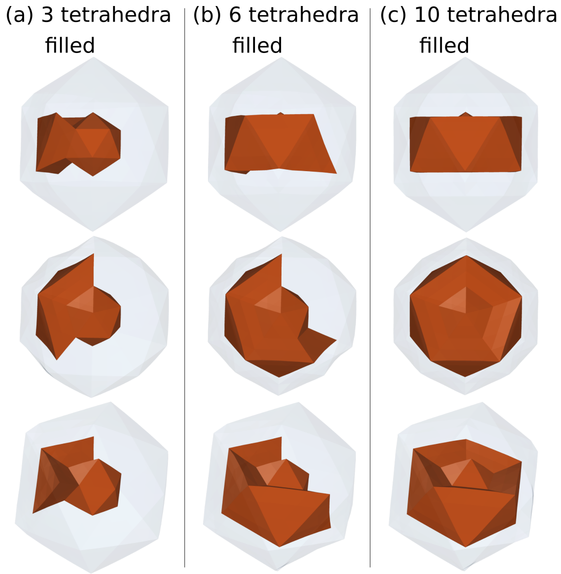

Figure 6: Filling of Cu during simulated annealing of an icosahedral Ag–Cu particle with 561 atoms. The constituent tetrahedra are filled sequentially (a–b) until a complete Cu ring of ten tetrahedra has been formed (c). The three rows show the same particles but from different angles.

For larger sizes, the icosahedral motif becomes increasingly unfavourable as a result of strain. Truncated decahedral particles, consisting of five truncated tetrahedra sharing a common edge, exhibit significantly less strain while still maintaining a large fraction of $\{111\}$ surfaces. As opposed to icosahedral particles, the core is not significantly more compressed than other parts of the particle (Fig. 5b, top row) and thus Cu does not preferentially fill the core as observed in icosahedral particles. Instead, Cu initially segregates around the fivefold axis near the apex, in layers close to yet excluding the actual surface (Fig. 5b, second row). Thereafter, Cu fills twin boundaries between the constituent tetrahedra (Fig. 5b, third row), and then segregates into one of the tetrahedra at a time (Fig. 5b, fourth row). The result is an off-center Cu core, the shape of which is largely governed by the underlying structure.

Truncated octahedra (Fig. 5c), i.e. single crystalline FCC polyhedra, are always the most stable motif for large enough size.[46] Of the three structures discussed here, it is the least compressed in the core and thus resembles decahedra in the sense that the Cu starts to segregate asymmetrically, close to the surface (Fig. 5c, second row). Just as for the other shapes, we find segregation to be highly anisotropic (Fig. 5c, third and fourth row), and we note once again that the Cu core is typically not spherical but quite irregular and faceted, with $\{111\}$ facets dominating. “Core–shell” is thus a crude simplification of the structure of these particles.

To summarize, minimization of surface energy, strain energy and the interface area between Ag and Cu all play important roles for the segregation behavior in Ag–Cu particles, but their importance vary depending on the underlying structure.

Conclusions

In this contribution, we have shone light on the interplay between bulk, surface and strain effects and how they impact equilibrium chemical ordering in Au–Pd and Ag–Cu nanoparticles. As expected, a strong tendency for surface segregation was observed in both systems. In Au–Pd, this results in segregation also in subsurface layers, driven by the favorable interaction between unlike atoms. Equilibrium chemical configurations are very similar regardless of structural motif, indicating that strain is of little importance in this system. In contrast, segregation in Ag–Cu is strongly influenced by the underlying structural motif and specifically the associated strain. In particular in particles with twin boundaries one observes a sequential "switching" of different parts of the nanoparticle. Asymmetric core structures that have been reported previously for this system appear naturally along such pathways. The notion of a core surrounded by a shell may be misleading, since the shape of the segregate is dictated by the structural motif, with the interface between the elements often coinciding with twin boundaries. We hope that future experiments can support or disregard these claims. It is, however, extraordinarily difficult to observe these effects experimentally, and only recently has atomic electron tomography been pushed to the resolution that would enable corroboration of our predictions.[48]

The composition of the surface is of great importance in many technological applications, including catalysis and plasmonics. Our results expose potential pitfalls: even if the surface composition is relatively predictable based on surface energies, the subsurface composition is not. One may find that it is heavily enriched in the element that does not segregate at the surface, as in Au–Pd, or that its composition has a dependency on the structural motif, as in Ag–Cu. This should be kept in mind when using surface sensitive experimental techniques such as X-ray photoelectron spectroscopy that probe more than just the topmost atomic layer – the surface segregation may be more pronounced than the experimental data suggests.

Acknowledgement

This work was funded by the Knut and Alice Wallenberg Foundation, the Swedish Research Council (grant number 2015-04153), and the Swedish Foundation for Strategic Research. Computer time allocations by the Swedish National Infrastructure for Computing at C3SE (Göteborg), NSC (Linköping), and PDC (Stockholm) are gratefully acknowledged.

Supporting Information Available

Mixing energies for truncated decahedral and octahedral particles, concentration profiles for a wide range of sizes and shapes. Movies of simulation trajectory of icosahedral Ag–Cu with 561 and 5083 atoms. This material is available free of charge via the Internet at `http://pubs.acs.org/`.

References

(1) Ferrando, R.; Jellinek, J.; Johnston, R. L. Nanoalloys: From Theory to Applications of Alloy Clusters and Nanoparticles. *Chemical Reviews* **2008**, *108*, 845–910.

(2) Sankar, M.; Dimitratos, N.; Miedziak, P. J.; Wells, P. P.; Kiely, C. J.; Hutchings, G. J. Designing Bimetallic Catalysts For a Green and Sustainable Future. *Chemical Society Reviews* **2012**, *41*, 8099.

(3) Shan, S.; Petkov, V.; Yang, L.; Luo, J.; Joseph, P.; Mayzel, D.; Prasai, B.; Wang, L.; Engelhard, M.; Zhong, C.-J. Atomic-Structural Synergy for Catalytic CO Oxidation over Palladium–Nickel Nanoalloys. *Journal of the American Chemical Society* **2014**, *136*, 7140–7151.

(4) Gould, A. L.; Heard, C. J.; Logsdail, A. J.; Catlow, C. R. A. Segregation Effects on the Properties of $(AuAg)_{147}$. *Physical Chemistry – Chemical Physics* **2014**, *16*, 21049–21061.

(5) Weissker, H.-C.; Mottet, C. Optical Properties of Pure and Core-Shell Noble-Metal Nanoclusters from TDDFT: The Influence of the Atomic Structure. *Physical Review B* **2011**, *84*, 165443.

(6) Teeriniemi, J.; Melander, M.; Lipasti, S.; Hatz, R.; Laasonen, K. Fe–Ni Nanoparticles: A Multiscale First-Principles Study to Predict Geometry, Structure, and Catalytic Activity. *Journal of Physical Chemistry C* **2017**, *121*, 1667–1674.

(7) Lee, Y. W.; Kim, M.; Kim, Z. H.; Han, S. W. One-Step Synthesis of Au@Pd Core–Shell Nanooctahedron. *Journal of the American Chemical Society* **2009**, *131*, 17036–17037.

(8) Hong, J. W.; Lee, Y. W.; Kim, M.; Kang, S. W.; Han, S. W. One-Pot Synthesis and Electrocatalytic Activity of Octapodal Au–Pd Nanoparticles. *Chemical Communications* **2011**, *47*, 2553–2555.

(9) Yang, Y.; Zhang, Q.; Fu, Z.-W.; Qin, D. Transformation of Ag Nanocubes into Ag–Au Hollow Nanostructures with Enriched Ag Contents to Improve SERS Activity and Chemical Stability. *ACS Applied Materials and Interfaces* **2014**, *6*, 3750–3757.

(10) Wang, Y.; Hou, M. Ordering of Bimetallic Nanoalloys Predicted from Bulk Alloy Phase Diagrams. *Journal of Physical Chemistry C* **2012**, *116*, 10814–10818.

(11) Yan, Z.; Taylor, M. G.; Mascareno, A.; Mpourmpakis, G. Size-, Shape-, and Composition-Dependent Model for Metal Nanoparticle Stability Prediction. *Nano Letters* **2018**, *18*, 2696–2704.

(12) Berthier, F.; Maras, E.; Legrand, B. Phase Diagrams of Nanoalloys: Influence of Size and Morphology. *Physical Chemistry – Chemical Physics* **2015**, *17*, 28347–28353.

(13) Bochicchio, D.; Ferrando, R. Morphological Instability of Core-Shell Metallic Nanoparticles. *Physical Review B* **2013**, *87*, 1–13.

(14) Goh, J. Q.; Akola, J.; Ferrando, R. Geometric Structure and Chemical Ordering of Large AuCu Clusters: A Computational Study. *Journal of Physical Chemistry C* **2017**, *121*, 10809–10816.

(15) Calvo, F. Thermodynamics of Nanoalloys. *Physical Chemistry – Chemical Physics* **2015**, *17*, 27922–27939.

(16) Deng, L.; Hu, W.; Deng, H.; Xiao, S. Surface Segregation and Structural Features of Bimetallic Au–Pt Nanoparticles. *Journal of Physical Chemistry C* **2010**, *114*, 11026–11032.

(17) Xiong, S.; Qi, W.; Huang, B.; Wang, M. Size-, Shape- and Composition-Dependent Alloying Ability of Bimetallic Nanoparticles. *ChemPhysChem* **2011**, *12*, 1317–1324.

(18) Pohl, J.; Stahl, C.; Albe, K. Size-Dependent Phase Diagrams of Metallic Alloys: A Monte Carlo Simulation Study on Order-Disorder Transitions in Pt-Rh Nanoparticles. *Beilstein Journal of Nanotechnology* **2012**, *3*, 1–11.

(19) Peng, L.; Ringe, E.; Van Duyne, R. P.; Marks, L. D. Segregation in Bimetallic Nanoparticles. *Physical Chemistry – Chemical Physics* **2015**, *17*, 27940–27951.

(20) Ringe, E.; Van Duyne, R. P.; Marks, L. D. Wulff Construction for Alloy Nanoparticles. *Nano Letters* **2011**, *11*, 3399–3403.

(21) Guisbiers, G.; Mendoza-Cruz, R.; Bazán-Díaz, L.; Velázquez-Salazar, J. J.; Mendoza-Perez, R.; Robledo-Torres, J. A.; Rodriguez-Lopez, J. L.; Montejano-Carrizales, J. M.; Whetten, R. L.; José-Yacamán, M. Electrum, the Gold-Silver Alloy, from the Bulk Scale to the Nanoscale: Synthesis, Properties, and Segregation Rules. *ACS Nano* **2016**, *10*, 188–198.

(22) Guisbiers, G.; Mendoza-Pérez, R.; Bazán-Díaz, L.; Mendoza-Cruz, R.; Velázquez-Salazar, J. J.; José-Yacamán, M. Size and Shape Effects on the Phase Diagrams of Nickel-Based Bimetallic Nanoalloys. *Journal of Physical Chemistry C* **2017**, *121*, 6930–6939.

(23) Peng, L.; Van Duyne, R. P.; Marks, L. D. Strain-Induced Segregation in Bimetallic Multiply Twinned Particles. *The Journal of Physical Chemistry Letters* **2015**, *6*, 1930–1934, PMID: 26263272.

(24) Gould, A. L.; Rossi, K.; Catlow, C. R. A.; Baletto, F.; Logsdail, A. J. Controlling Structural Transitions in AuAg Nanoparticles through Precise Compositional Design. *Journal of Physical Chemistry Letters* **2016**, *7*, 4414–4419.

(25) Aslan, M.; Davis, J. B. A.; Johnston, R. L. Global Optimization of Small Bimetallic Pd-Co Binary Nanoalloy Clusters: A Genetic Algorithm Approach at the DFT Level. *Physical Chemistry – Chemical Physics* **2016**, *18*, 6676–6682.

(26) Heiles, S.; Johnston, R. L. Global Optimization of Clusters Using Electronic Structure Methods. *International Journal of Quantum Chemistry* **2013**, *113*, 2091–2109.

(27) Kovács, G.; Kozlov, S. M.; Neyman, K. M. Versatile Optimization of Chemical Ordering in Bimetallic Nanoparticles. *Journal of Physical Chemistry C* **2017**, *121*, 10803–10808.

(28) Palomares-Baez, J.-P.; Panizon, E.; Ferrando, R. Nanoscale Effects on Phase Separation. *Nano Letters* **2017**, *17*, 5394–5401.

(29) Chatzidakis, M.; Prabhudev, S.; Saidi, P.; Chiang, C. N.; Hoyt, J. J.; Botton, G. A. Bulk Immiscibility at the Edge of the Nanoscale. *ACS Nano* **2017**, *11*, 10984–10991.

(30) Delfour, L.; Creuze, J.; Legrand, B. Exotic behavior of the outer shell of bimetallic nanoalloys. *Physical Review Letters* **2009**, *103*, 205701.

(31) Akbarzadeh, H.; Mehrjouei, E.; Shamkhali, A. N.; Abbaspour, M.; Salemi, S.; Ramezanzadeh, S. Au@void@AgAu Yolk-Shell Nanoparticles with Dominant Strain Effects: A Molecular Dynamics Simulation. *Journal of Physical Chemistry Letters* **2017**, *8*, 5064–5068.

(32) Ferrando, R. Symmetry Breaking and Morphological Instabilities in Core-Shell Metallic Nanoparticles. *Journal of Physics Condensed Matter* **2015**, *27*, 013003.

(33) Atanasov, I.; Ferrando, R.; Johnston, R. L. Structure and Solid Solution Properties of Cu–Ag Nanoalloys. *Journal of Physics Condensed Matter* **2014**, *26*, 275301.

(34) Laasonen, K.; Panizon, E.; Bochicchio, D.; Ferrando, R. Competition Between Icosahedral Motifs in AgCu, AgNi, and AgCo Nanoalloys: A Combined Atomistic-DFT Study. *Journal of Physical Chemistry C* **2013**, *117*, 26405–26413.

(35) Sadigh, B.; Erhart, P.; Stukowski, A.; Caro, A.; Martinez, E.; Zepeda-Ruiz, L. Scalable Parallel Monte Carlo Algorithm for Atomistic Simulations of Precipitation in Alloys. *Physical Review B* **2012**, *85*, 184203.

(36) Sadigh, B.; Erhart, P. Calculation of Excess Free Energies of Precipitates via Direct Thermodynamic Integration Across Phase Boundaries. *Physical Review B* **2012**, *86*, 134204.

(37) Plimpton, S. Fast Parallel Algorithms for Short-Range Molecular Dynamics. *Journal of Computational Physics* **1995**, *117*, 1–19.

(38) Mishin, Y.; Mehl, M. J.; Papaconstantopoulos, D. A.; Voter, A. F.; Kress, J. D. Structural Stability and Lattice Defects in Copper: Ab Initio, Tight-Binding, and Embedded-Atom Calculations. *Physical Review B* **2001**, *63*, 224106.

(39) Williams, P. L.; Mishin, Y.; Hamilton, J. C. An Embedded-Atom Potential for the Cu–Ag System. *Modelling and Simulation in Materials Science and Engineering* **2006**, *14*, 817–833.

(40) Marchal, R.; Genest, A.; Krüger, S.; Rösch, N. Structure of Pd/Au Alloy Nanoparticles from a Density Functional Theory-based Embedded-Etom Potential. *Journal of Physical Chemistry C* **2013**, *117*, 21810–21822.

(41) Stukowski, A. Visualization and Analysis of Atomistic Simulation Data with OVITO–the Open Visualization Tool. *Modelling and Simulation in Materials Science and Engineering* **2010**, *18*, 015012.

(42) Subramanian, P. R.; Perepezko, J. H. The Ag–Cu (Silver-Copper) System. *J. Phase Equilib.* **1993**, *14*, 62–75.

(43) Okamoto, H.; Massalski, T. B. The Au–Pd (Gold-Palladium) System. *Bull. Alloy Phase Diagrams* **1985**, *6*, 229–235.

(44) Tyson, W.; Miller, W. Surface Free Energies of Solid Metals: Estimation from Liquid Surface Tension Measurements. *Surface Science* **1977**, *62*, 267 – 276.

(45) Li, C.; Raciti, D.; Pu, T.; Cao, L.; He, C.; Wang, C.; Mueller, T. Improved Prediction of Nanoalloy Structures by the Explicit Inclusion of Adsorbates in Cluster Expansions. *Journal of Physical Chemistry C* **2018**,

(46) Rahm, J. M.; Erhart, P. Beyond Magic Numbers: Atomic Scale Equilibrium Nanoparticle Shapes for Any Size. *Nano Letters* **2017**, *17*, 5775–5781.

(47) Narayan, T. C.; Baldi, A.; Koh, A. L.; Sinclair, R.; Dionne, J. A. Reconstructing Solute-Induced Phase Transformations within Individual Nanocrystals. *Nature Materials* **2016**, *15*, 768–774.

(48) Yang, Y.; Chen, C.-c.; Scott, M. C.; Ophus, C.; Xu, R.; Jr, A. P.; Wu, L.; Sun, F.; Theis, W.; Zhou, J. et al. Deciphering chemical order/disorder and material properties at the single-atom level. *Nature* **2017**, *542*, 75–79.

— Supporting Information —

Understanding Chemical Ordering in Bimetallic Nanoparticles from Atomic Scale Simulations: The Competition between Bulk, Surface and Strain

J. Magnus Rahm and Paul Erhart*

Chalmers University of Technology, Department of Physics, S-412 96 Gothenburg, Sweden

E-mail: erhart@chalmers.se

Mixing energy in truncated octahedral and decahedral particles

The mixing energy of truncated octahedral and decahedral particles of various sizes is shown in Fig. S1. The behavior is very similar to the one of icosahedral particles as presented in Fig. 1 of the main paper.

Mixing energy with pure particles as references

Figures 1 and S1 both show the mixing energy with the pure bulk phases as references, i.e.

$$E_{\mathrm{mix}} = E_{\mathrm{A\text{–}B}} - cE_{\mathrm{A}}^{\mathrm{bulk}} - (1-c)E_{\mathrm{B}}^{\mathrm{bulk}}. \tag{1}$$

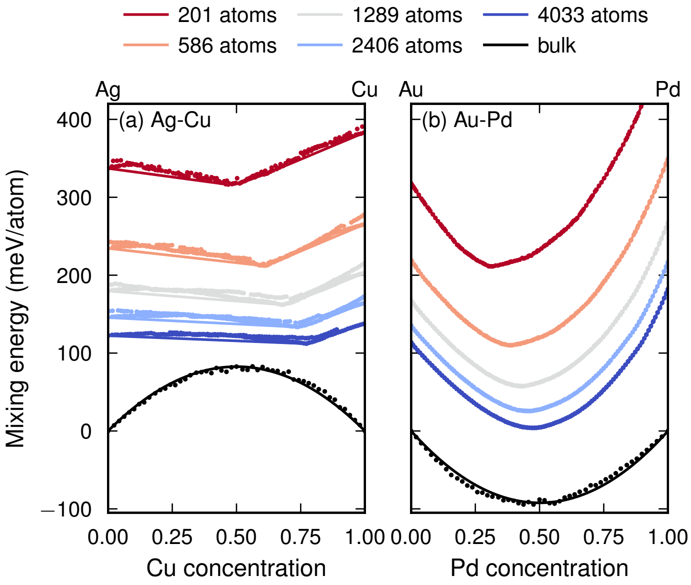

(a) Regular truncated octahedra

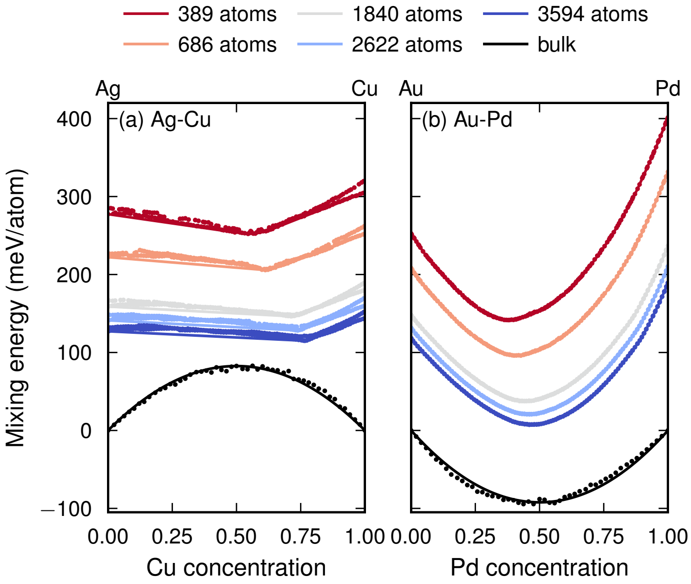

(b) Trunated decahedra

Figure S1: Mixing energy in (a) regular truncated octahedra and (b) truncated decahedra of various sizes, compared to mixing energy in bulk systems. Two simulations were carried out for each size, one starting with pure Ag/Au and ending with pure Cu/Pd and one in the opposite direction.

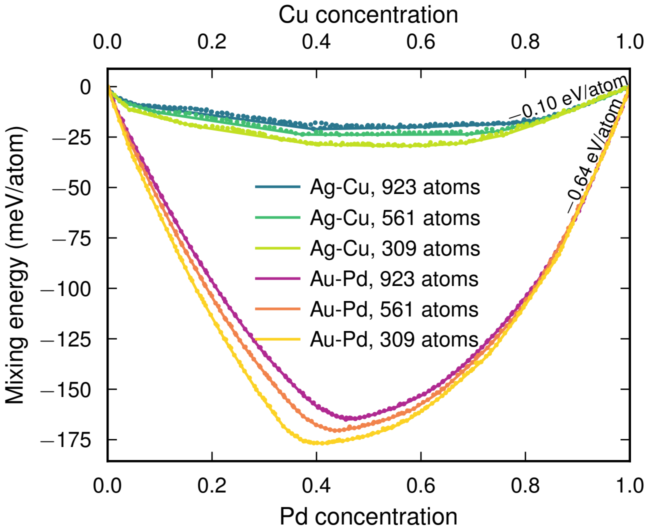

Figure S2: Mixing energy with the pure *particles* as references. In both Au–Pd and Ag–Cu, the energy gain of adding an Au/Ag atom to an otherwise pure Pd/Cu atom is independent of particle size.

One can also define a mixing energy in which the energies of the elemental particles are used as reference (Fig. S2), i.e.

$$\widetilde{E}_{\mathrm{mix}} = E_{\mathrm{A\text{–}B}} - cE_{\mathrm{A}}^{\mathrm{particle}} - (1-c)E_{\mathrm{B}}^{\mathrm{particle}}. \tag{2}$$

This makes it evident that the energy of adding an Au/Ag atom to an otherwise pure Pd/Cu particle is constant with respect to particle size for both Au–Pd and Ag–Cu. Inspection of the trajectories reveals that such atoms always reside in the surface of the particle.

Surface segregation in a Au–Pd slab

The concentration in the topmost four layers of an Au–Pd slab, as a function of the concentration of Pd in the bulk, is shown in Fig. S3. Atomic layers that are sufficiently deep in the slab approach the diagonal, which represents a composition in the atomic layer that equals the one of the slab as a whole. Close to the surface, the concentration deviates significantly from the diagonal, meaning that segregation has occurred. Note that the odd layers (layer

1 and 3) are to the lower right of the diagonal, signifying that they are always richer in Au than the interior of the slab, whereas the first even layer (layer 2) is on the opposite side, signifying enrichment in Pd.

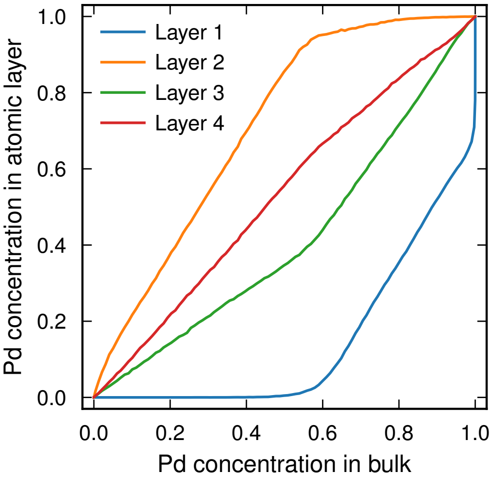

Figure S3: Concentration per atomic layer in a 25 layer Au–Pd slab at 300 K as a function of bulk concentration (i.e., the concentration in the innermost seven atomic layers) obtained from a MD/MC simulation in which the concentration was swept over the whole range. Layer 1 is the surface layer, layer 2 the first subsurface layer, etc.

Concentration profiles

Sampling of the full concentration range at 300 K was performed for icosahedra of eight different sizes (Fig. S4), regular truncated octahedra of five sizes (Fig. S5) and decahedra of five sizes (Fig. S6). The decahedra were chosen with a truncation leading to a particularly low energy for the materials at hand.

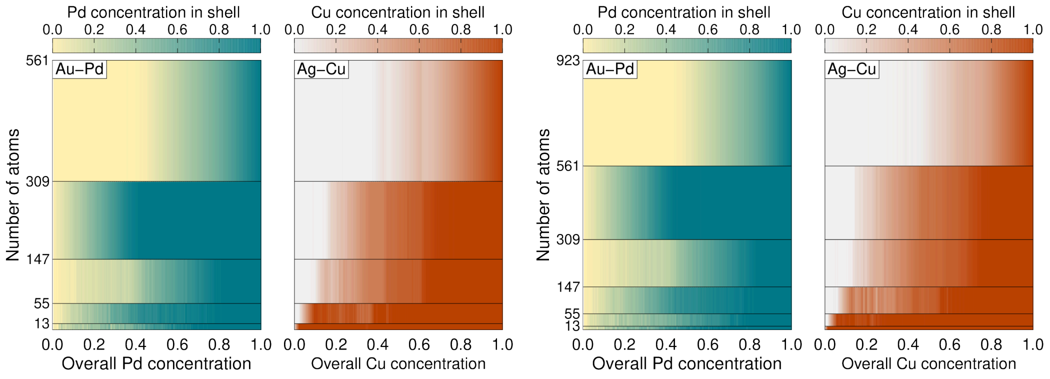

(a) 561 atoms (b) 923 atoms

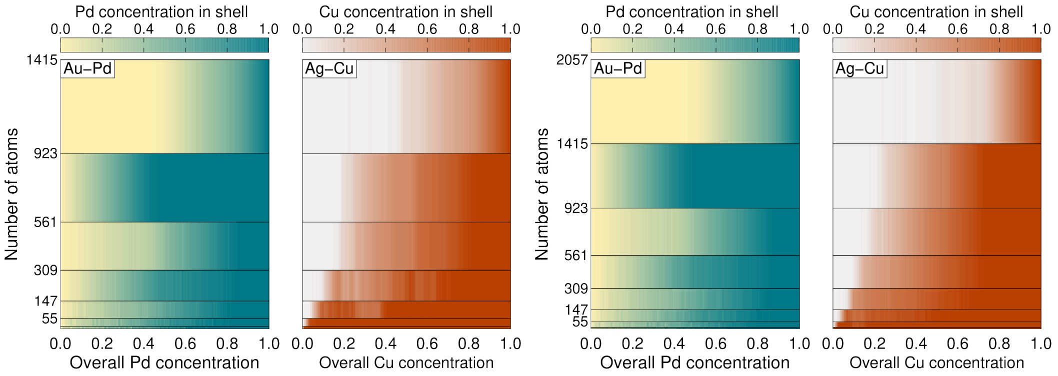

(c) 1415 atoms (d) 2057 atoms

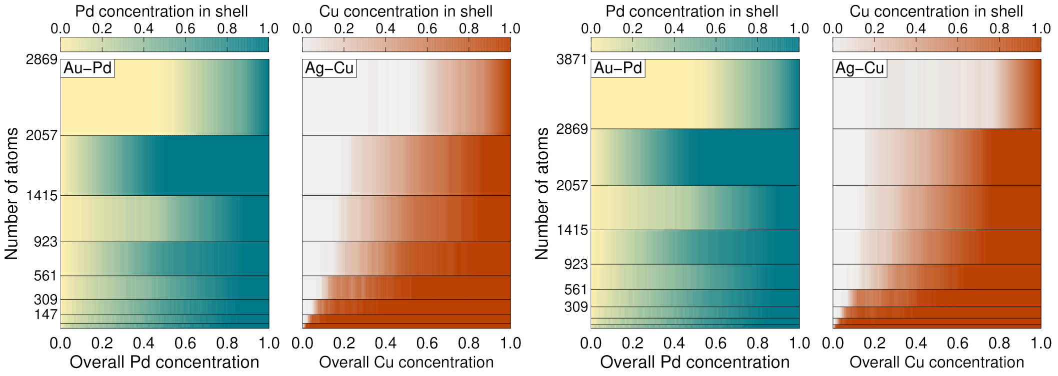

(e) 2869 atoms (f) 3871 atoms

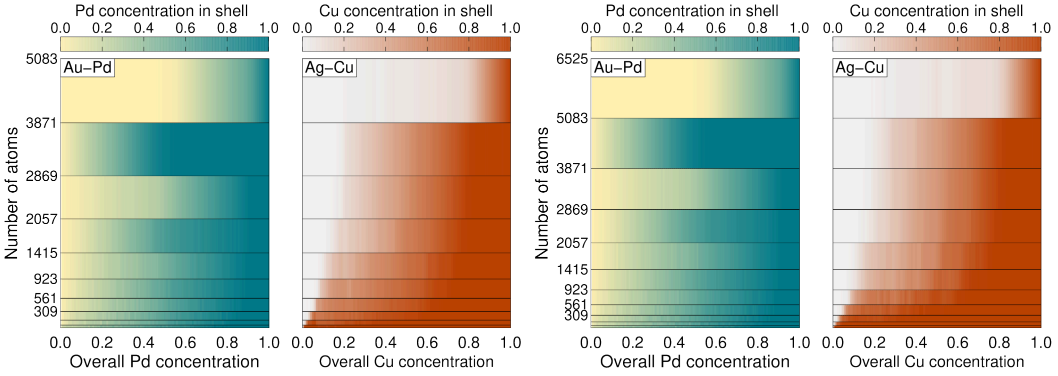

(g) 5083 atoms (h) 6525 atoms

Figure S4: Average concentration at 300 K in isosahedral particles, ordered by atomic shell with core at the bottom and surface at the top. Figure (g) is the same as in the main paper. The horizontal axes represent the overall Pd/Cu concentration in the particle as a whole whereas the color scale represent the concentration in each shell specifically.

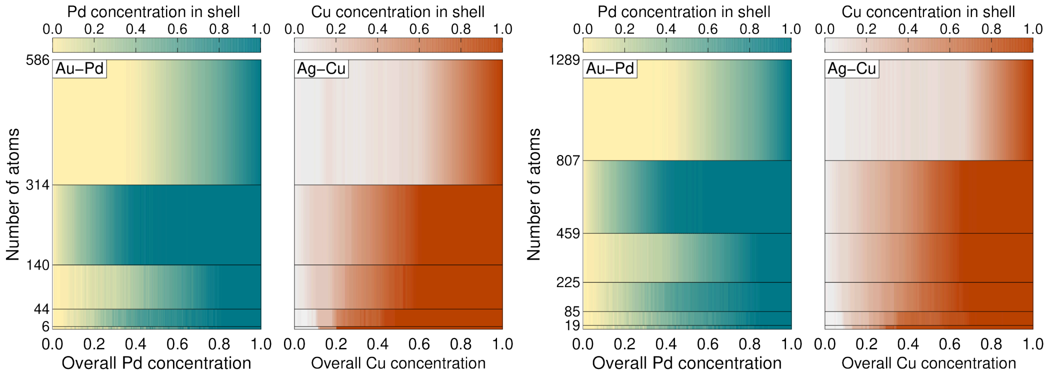

(a) 586 atoms

(b) 1289 atoms

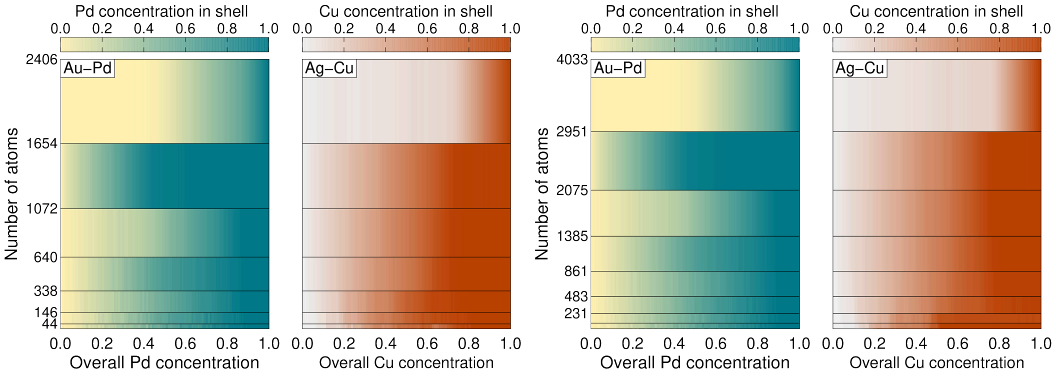

(c) 2406 atoms

(d) 4033 atoms

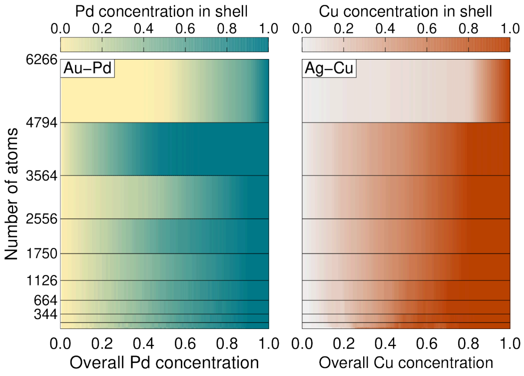

(e) 6266 atoms

Figure S5: Average concentration at 300 K in regularly truncated octahedral particles, ordered by atomic shell with core at the bottom and surface at the top. The horizontal axes represent the overall Pd/Cu concentration in the particle as a whole whereas the color scale represent the concentration in each shell specifically.

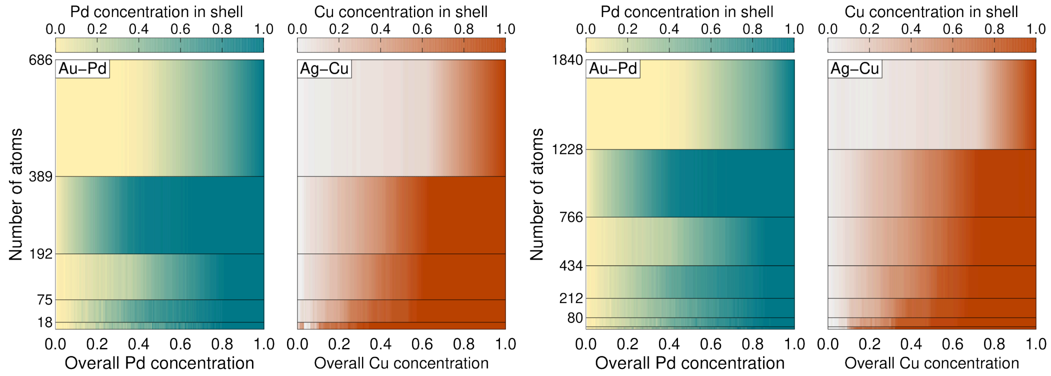

(a) 686 atoms (b) 1840 atoms

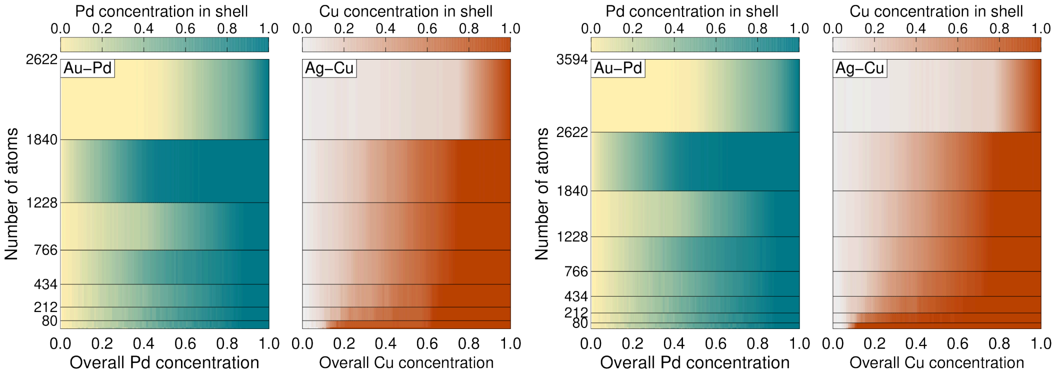

(c) 2622 atoms (d) 3594 atoms

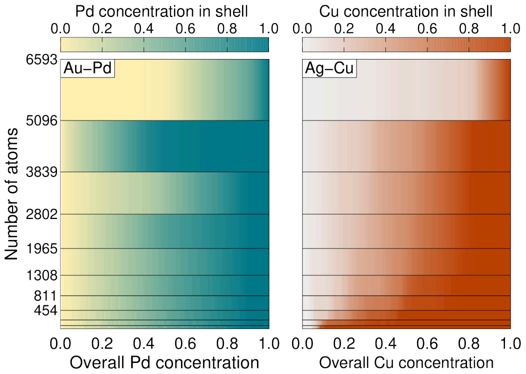

(e) 6593 atoms

Figure S6: Average concentration at 300 K in truncated decahedral particles, ordered by atomic shell with core at the bottom and surface at the top. The horizontal axes represent the overall Pd/Cu concentration in the particle as a whole whereas the color scale represent the concentration in each shell specifically.